JCI The Journal of Clinical Investigation

Blocking p62/SQSTM1-dependent SMN degradation ameliorates Spinal Muscular Atrophy disease phenotypes

Natalia Rodriguez-Muela, … , Rajat Singh, Lee L. Rubin

J Clin Invest. 2018. https://doi.org/10.1172/JCI95231.

Research Article Neuroscience Stem cells

Spinal muscular atrophy (SMA), a degenerative motor neuron (MN) disease caused by loss of functional SMN protein due to *SMN1* gene mutations, is a leading cause of infant mortality. Increasing SMN levels ameliorates the disease phenotype and is unanimously accepted as a therapeutic approach for SMA patients. The ubiquitin/proteasome system is known to regulate SMN protein levels; however whether autophagy controls SMN levels remains poorly explored. Here we show that SMN protein is degraded by autophagy. Pharmacological and genetic inhibition of autophagy increase SMN levels, while induction of autophagy decreases SMN. SMN degradation occurs via its interaction with the autophagy adapter p62/SQSTM1. We also show that SMA neurons display reduced autophagosome clearance, increased p62/ubiquitinated protein levels, and hyperactivated mTORC1 signaling. Importantly, reducing p62 levels markedly increases SMN and its binding partner gemin2, promotes MN survival and extends lifespan in fly and mouse SMA models revealing p62 as a new potential therapeutic target to treat SMA.

Blocking p62/SQSTM1-dependent SMN degradation ameliorates Spinal Muscular Atrophy disease phenotypes

Correspondence information for corresponding authors:

Natalia Rodriguez-Muela

7 Divinity Avenue
Sherman Fairchild G53
Cambridge, MA 02138
Email: natalia_rodriguezmuela@harvard.edu
Ph: (617) 384-8105

Lee L. Rubin

7 Divinity Avenue
Sherman Fairchild G60
Cambridge, MA 02138
Email: lee_rubin@harvard.edu
Ph: (617) 384-8105

CONFLICT OF INTERESTS

The Authors declare no relevant conflict of interests.

Blocking p62/SQSTM1-dependent SMN degradation ameliorates Spinal Muscular Atrophy disease phenotypes

Natalia Rodriguez-Muela[1,2*], Andrey Parkhitko[3#], Tobias Grass[1,2#], Rebecca M. Gibbs[1,2], Erika M. Norabuena[1,2], Norbert Perrimon[3,4], Rajat Singh[5], Lee L. Rubin[1,2*]

[1]Department of Stem Cell and Regenerative Biology, Harvard University, Cambridge, Massachusetts, USA

[2] Harvard Stem Cell Institute, Harvard University, Cambridge, Massachusetts, USA

[3] Department of Genetics, Harvard Medical School, Boston, Massachusetts, USA

[4]Howard Hughes Medical Institute, Boston, Massachusetts 02115, USA

[5]Department of Medicine; Albert Einstein College of Medicine; Bronx, NY, USA.

# These authors contributed equally to this work

*Corresponding authors: natalia_rodriguezmuela@harvard.edu, lee_rubin@harvard.edu; phone: (617) 384-8105

Abstract

Spinal muscular atrophy (SMA), a degenerative motor neuron (MN) disease caused by loss of functional SMN protein due to *SMN1* gene mutations, is a leading cause of infant mortality. Increasing SMN levels ameliorates the disease phenotype and is unanimously accepted as a therapeutic approach for SMA patients. The ubiquitin/proteasome system is known to regulate SMN protein levels; however whether autophagy controls SMN levels remains poorly explored. Here we show that SMN protein is degraded by autophagy. Pharmacological and genetic inhibition of autophagy increase SMN levels, while induction of autophagy decreases SMN. SMN degradation occurs via its interaction with the autophagy adapter p62/SQSTM1. We also show that SMA neurons display reduced autophagosome clearance, increased

p62/ubiquitinated protein levels, and hyperactivated mTORC1 signaling. Importantly, reducing p62 levels markedly increases SMN and its binding partner gemin2, promotes MN survival and extends lifespan in fly and mouse SMA models revealing p62 as a new potential therapeutic target to treat SMA.

Introduction

SMA is an early-onset, autosomal recessive neuromuscular disease caused by low levels of SMN protein (1). SMA is primarily characterized by degeneration of motor neurons (MNs) of the spinal cord and skeletal muscle atrophy. However, recent studies have revealed a wide range of pathologies in multiple peripheral tissues in humans and mice (2). Due to a gene duplication event, humans harbor 0-6 copies of *SMN2*, a paralog to *SMN1*. A single nucleotide difference between *SMN1* and *SMN2* leads to alternative splicing of *SMN2* (3, 4). While *SMN1* primarily produces full-length SMN (SMN-FL) transcript, ~90% of the *SMN2* gene product lacks exon 7 (SMN-Δ7), a highly unstable form of the protein (5, 6). *SMN2* is a major SMA disease modifier, with higher *SMN2* copy number correlating with delayed disease onset and better prognosis. SMN is ubiquitously expressed, localized in the cytoplasm and nuclear foci termed gems, and plays an essential housekeeping role in biogenesis of spliceosomal small nuclear ribonucleoprotein particles (snRNPs) (7) and axonal transport of mRNA (8). A large body of evidence suggests that increasing SMN levels repairs the disease phenotype. Although a number of compounds that increase SMN levels by stimulating its transcription or altering the *SMN2* splicing pattern have been identified (9-14), SMN is also regulated at the level of protein degradation. We and others have shown that SMN protein is degraded by the ubiquitin-proteasome system (UPS) (15-20). However, the role of macroautophagy (hereafter autophagy) in regulating SMN protein levels has not been investigated. Autophagy is a highly conserved intracellular degradative pathway that eliminates cell components to maintain cellular homeostasis (21). While the proteasome degrades short-lived proteins, autophagy turns over damaged, redundant and aggregated proteins, as well as cellular organelles, in-bulk but also in a selective manner due to a number of proteins, called autophagy receptors, that specifically recognize certain cargo and deliver it to autophagosomes (APs) for degradation (22, 23). The role of autophagy in neurodegenerative disorders has been extensively investigated (24-28). However, its contribution to the pathophysiology of SMA remains unknown.

Here we demonstrate that SMN protein levels are regulated by autophagy. We show that lysosomal inhibition increases levels of total SMN protein, ubiquitinated SMN, SMN-binding partner gemin2 and the number of nuclear gems as well as levels of partially functional SMN-Δ7. We also show that SMN degradation is mediated by its ubiquitination and interaction with the autophagy receptor p62/SQSTM1 (hereafter p62). Our study unravels a highly activated mTOR pathway in SMA affected cells that contributes to the deficient AP clearance and subsequent accumulation of ubiquitinated proteins and p62. Importantly, depleting p62 levels markedly rescues MN death *in vitro* and extends lifespan of SMA fly and mouse models. Taken together, our results suggest new therapeutic possibilities for treatment of SMA by dampening autophagy-dependent SMN degradation.

Results

Autophagy regulates SMN protein levels

Restoring SMN protein levels above a certain threshold is the most common approach to treating SMA. While SMN protein levels are controlled at transcriptional and post-transcriptional levels, in the last few years therapeutic strategies have focused primarily on transcriptional regulation of SMN. It is thought that SMN degradation occurs mainly via the UPS (15-20). However, since SMN is part of large multi-protein complexes including the SMN complex, formed by SMN and gemins (2-8) (key components of spliceosomes) (7), stress granules (29) and axonal granules involved in axonal transport (8), we wondered whether degradation of SMN occurred in bulk as part of these large protein complexes via autophagy.

To determine whether autophagy regulates SMN degradation, we first exposed human fibroblasts to the best-known autophagy inducer, starvation, by depriving them of serum (S-), and blocked lysosomal degradation by exposing cells to lysosomal inhibitors (ammonium chloride and leupeptin, NL). We observed that, not only did SMN levels decrease with serum starvation, but, importantly, SMN levels were elevated when autophagy activity was blocked (Figure 1A-B) indicating that SMN is degraded via autophagy. We also wished to determine whether autophagy controls SMN protein levels in MNs, the most severely affected cell type in the disease. Given that autophagy is not efficiently triggered by starvation in neurons (21), we reduced the expression of a crucial gene required for autophagosome formation, *Atg7*, in mouse embryonic stem cell (ESC)-derived MNs by shRNA delivery. As expected, we observed that

MNs with reduced Atg7 showed increased levels of the autophagy substrate p62, accumulation of ubiquitinated proteins, as well as reduced levels of the AP marker LC3-II (Figure 1C). As we had anticipated, we also noted an increase in levels of SMN when compared to control cultures (NS) (Figure 1C) confirming that autophagy meditates SMN degradation. It is traditionally accepted that, upon ubiquitination, SMN degradation occurs solely via the UPS. Our results led us to explore whether ubiquitinated-SMN is also degraded by autophagy. In fact, when HA-SMN-FL-expressing HEK293T cells were treated with modulators of autophagy (inhibitors: NL and weak base hydroxychloroquine (HCQ); and a well-known activator of autophagy, rapamycin) or the proteasome inhibitor MG132 and subjected to immunoprecipitation (IP) using an anti-HA antibody, there was accumulation of ubiquitinated-SMN upon both proteasomal and lysosomal blockage (Figure 1D).

Given these findings, we next determined whether the truncated form of SMN protein, SMN-Δ7, is also an autophagy substrate. Cells from SMA patients express higher levels of SMN-Δ7 than SMN-FL. Although SMN-Δ7 is highly unstable, it retains some function, at least in the presence of SMN-FL (5, 6, 30). While it has been reported that SMN-Δ7 is quickly degraded by the proteasome (16), its oligomerization with SMN-FL increases its stability (30). Because SMN-Δ7 binds to SMN-FL, we postulated that SMN-Δ7 might also be degraded by autophagy. To answer this question, we transfected HEK293T cells with HA-tagged forms of both proteins and we induced autophagy by subjecting them to amino acid starvation (EBSS media), to rapamycin or both. Indeed, induction of autophagy led to decreased levels of SMN-FL and SMN-Δ7, which were more pronounced upon combining both autophagy-inducing stimuli (Figure 1E) demonstrating that SMN-Δ7 protein levels are also under autophagy control. Interestingly, levels of gemin2, an SMN binding protein and essential spliceosome component, were also decreased upon autophagy induction (with serum starvation, S-), and increased upon lysosomal inhibition (NL) (Figure 1F). Taken together, these data demonstrate that autophagy degrades ubiquitinated-SMN and other components of the SMN complex, e.g., gemin2, which in turn suggests that the pool of SMN degraded by autophagy is the one associated with SMN complexes.

SMN degradation by autophagy is mediated by p62

Autophagy is not only an in-bulk catabolic process; it also selectively targets specific substrates for degradation. Several autophagy cargo-recognition proteins, or autophagy receptors, have been identified, including p62, NBR1, optineurin, NDP52 and NIX (22, 23). They share key domains that allow binding to autophagic cargo for their delivery for lysosomal degradation. Through their ubiquitin-binding domain (UBA motif) these receptors bind to polyubiquitinated cargo, and via their LC3-binding domain (LC3-interacting-region or LIR motif) they interact with LC3 that coats the inner membrane of autophagosomes (22, 31-33). These proteins are also autophagy substrates, and hence, serve as markers for autophagy flux.

To investigate whether autophagy receptors mediate SMN degradation, we focused first on the best-characterized autophagy receptor, p62. Depleting p62 levels with shRNAs markedly increased SMN protein levels in wildtype mouse MNs (Figure 2A), without increasing SMN mRNA expression levels (Figure S1A). These results led us to explore if the same was true in SMA MNs. We obtained ESCs from a severe SMA mouse model, SMNΔ7, in which *Smn* has been deleted, and two copies of the human *SMN2* transgene and two copies of the human *SMN2* transgene lacking exon 7 have been inserted into the genome (*Smn-/-;SMN2+/+*;SMNΔ7+/+;*Hb9::GFP*)(30). SMN protein levels in both ESCs and MNs derived from these mice are reduced by ~70% when compared to wildtype controls (Figure S1B-C). Knocking-down p62 in SMNΔ7 MNs led to increases in SMN protein levels similar to those observed in wildtype MNs (Figure 2A).

We also studied the number of nuclear gems. Gems are multiprotein nuclear structures composed of SMN molecules, gemins2-7 and snRNPs involved in the transcription and processing of many types of nuclear RNAs (7). Reduction of their number per cell is an SMA hallmark. Interestingly, p62 down-regulation led to an increase in the number of gemin2^{+} and SMN^{+} nuclear gems in SMA MNs and also in other neurons in the culture (non-MN population) (Figure 2B and S1D). This finding led us to explore whether the effect of p62 depletion on increases in SMN protein levels is more marked in the nucleus than in the cytoplasm. However, cellular fractionation assays of p62 knocked-down NIH3T3 cells, that also exhibited significantly higher SMN levels in total lysates when compared to NS control (Figure S1E), showed similar increases in SMN and gemin2 levels in both cellular fractions, which indicates that stabilization of these proteins occurs in both the nucleus and cytoplasm (Figure 2C-D).

We extended these results by showing that p62 regulates SMN protein levels in human MNs. We derived MNs from induced pluripotent stem cells (iPSCs) from healthy control and SMA patients affected by different disease severities – a severe line (type II, I-51C) and a very severe line (type I, I-38G) – that we have previously described (34, 35). These iPSCs and the derived MNs express amounts of SMN that reflect their disease severities (35). Similar to what we observed in mouse MNs, depleting p62 levels in human MNs also led to an increase in SMN protein levels (Figure 2E-F, S1F). To verify the importance of p62 as a mediator of SMN degradation, we studied SMN protein levels in brains from adult p62 null mice. Confirming our results, brains from heterozygous and p62 null mice showed markedly increased SMN protein levels when compared to littermate controls (Figure 2G-H). Together, these data indicate that p62 regulates SMN and gemin2 protein levels in all cell types studied, including human control and SMA iPSC-derived MNs and in mice.

p62 interacts with SMN

Given our findings, we next explored how p62 functions as an autophagy receptor to target SMN for degradation. We performed co-IP analysis after transfecting HEK293T cells with HA-SMN and myc-p62 or various combinations of plasmids used as negative controls (HA-GFP + myc-p62 and HA-SMN + myc-E2-crimson, a far-red fluorescent protein). We observed that, while myc-p62 IP did not pull down HA-SMN, HA-SMN did co-immunoprecipitate with myc-p62 (Figure 3A). Co-IPs of HA-GFP with myc-p62 and of HA-SMN with myc-E2-crimson were negative as we expected (Figure 3A). These results indicate that SMN and p62 indeed interact with one another. To confirm these data, we performed IP of endogenous proteins in mouse MNs. Interestingly we did not detect interaction between SMN and p62 under basal conditions. However, binding of SMN to p62 was detected when we induced the incorporation of SMN into protein complexes. It has been reported that besides being distributed throughout the cytoplasm and localizing to the nucleus when assembled into gems, SMN can also cluster in cytoplasmic structures called stress granules (SG) in response to oxidative stress (29). SGs are mainly composed of RNA-binding proteins such as Tia1, TIAR, FUS and SMN among others (29, 36) and mRNA, and their main function is to prevent translation of mRNA during cellular stress (29). To test whether p62 interacts with SMN in SGs, we induced oxidative stress in HEK293T cells transfected with combinations of constructs described above by exposing them to 10 and 50

μM sodium arsenite (NaAsO; SA) for 6 hours, a commonly used method to induce SG formation. We observed that HA-SMN strongly co-immunoprecipitated with myc-p62 upon SG formation (Figure S2A).

To explore the reproducibility of these findings with endogenous proteins, we subjected mouse SMA MNs to similar analyses. Importantly, upon treatment with SA, endogenous SMN co-immunoprecipitated with p62 (Figure 3B). Interestingly, in wildtype MNs, exposure to SA resulted in a lower ratio of immunoprecipitated SMN to SMN in total lysates when compared to controls (Figure S2B). By contrast, in SMA MNs, this difference was not as pronounced, indicating that upon SA-induced SG formation, the pool of SMN present in SG (therefore not available in protein lysates due to their incorporation in large aggregates and not extracted by a mild lysis detergent) is possibly larger in wildtype cells than in SMA MNs. These results agree with previous studies reporting that SMN-deficient cells have impaired SG formation, which increases their susceptibility to death (37). Second, we noted that co-IP of SMN with p62 was more efficient in SMA MNs (Figure 3B) than wildtype MNs (Figure S2B) and that localization of p62 in aggregates upon SA treatment was more evident in SMA MNs (Figure 3C and S2C). Therefore, the incorporation of SMN in SGs, or SG formation itself, might be impaired in SMA cells; however, the interaction between SMN and p62 is enhanced in the diseased cells.

Recently published data from our lab suggest that SMN is ubiquitinated by Cullin5-E3 ubiquitin ligase (Cul5) targeting it for degradation and that over-expression of a dominant-negative (DN) form of Cul5 stabilizes SMN (35). We postulated that ubiquitinated-SMN could at least be a fraction of the SMN protein that is recognized by p62 and degraded via autophagy. To test this possibility, we infected mouse SMA and wildtype ESC-derived MNs with lentiviruses carrying Cul5DN or a control empty vector, and we exposed them to SA to induce the localization of SMN in stress granules. We performed SMN IP and, as expected, we observed that for both types of MNs the amount of pulled-down ubiquitinated-SMN after Cul5DN expression was reduced (Figure 3D-E). As a result, in wildtype MNs the interaction of SMN with p62 was reduced in Cul5DN-expressing MNs compared to empty-vector treated ones (Figure 3D). Interestingly, and in agreement with our previous results, the binding between SMN and p62 is still maintained after Cul5DN over-expression in SMA MNs. This again suggests that in the diseased cells the fraction of p62 that binds to SMN, at least under SG formation conditions, is larger, or p62-SMN interaction stronger, than in wildtype cells (Figure 3E). Taken

together, these data suggest that p62 interacts readily with the pool of SMN that is assembled in protein complexes. Furthermore, these data indicate that preventing SMN ubiquitination reduces its ability to bind p62.

SMN deficiency leads to autophagy failure and accumulation of p62/ubiquitinated proteins

Autophagy dysfunction has been widely described in multiple neurodegenerative diseases; however, its participation in the pathophysiology of SMA remains largely unexplored. Thus, we decided to investigate autophagy function in SMA cells. First, fibroblasts from patients with different SMA severities (type I, I-38; type II, I-51; and type III, I-39) showed higher levels of LC3-I and LC3-II than controls (Figure 4A and S3A), suggesting that autophagosome (AP) formation remains intact in SMA. To determine whether the increase in LC3-II represents an increase in AP formation and not a block in its fusion with lysosomes or its degradation, we studied autophagy flux by measuring LC3-II turnover in presence and absence of lysosomal inhibitors. If autophagy flux occurs properly, the amount of LC3-II should be higher in the presence of lysosomal inhibitors (38). In SMA fibroblasts, the increase in LC3-II following lysosomal blockage under control and starvation conditions was reduced when compared to control fibroblasts (Figure 4A), indicating a defect in autophagy flux. This was accompanied by increased p62 protein levels in SMA fibroblasts – a hallmark of autophagy blockage (Figure S3B). These data suggest that SMN deficiency impairs autophagy in human fibroblasts.

In order to validate these results, we explored whether a similar dysfunction in autophagy occurs in SMA MNs. Indeed, murine SMA MNs showed higher levels of p62 (while mRNA expression remained unchanged, Figure S3C) and ubiquitinated proteins compared to wildtype MNs, and higher levels of LC3-I and LC3-II (Figure 4B), which correlated with an increased LC3 immunostaining in MNs in culture (Figure S3D). We confirmed these results in human iPSC-derived MNs that showed higher levels of p62 and ubiquitinated proteins in SMA compared to healthy MNs (Figure 4C and S3E). To investigate how relevant these results from *in vitro* MNs are to the disease *in vivo*, we immunostained cervical spinal cord sections from SMNΔ7 mice and wildtype littermates for p62 and ubiquitin. In line with our *in vitro* results, we observed that Hb9:GFP^{+} ventral MNs from postnatal day 10 SMNΔ7 mice showed increased p62 and ubiquitin staining compared to wildtype MNs (Figure S3F). These results demonstrate that autophagy is impaired in MNs, both from mouse and human.

Autophagy can be dysregulated at several steps, and in the context of neurodegenerative diseases a growing number of studies have reported that alterations at each of these steps can lead to autophagy failure (39). Our results indicate that AP clearance is partially impaired in SMA cells. To further explore this possibility, we studied autophagy flux by using a mCherry-GFP-LC3 construct. This allows us to distinguish APs (both green and red giving rise to yellow puncta) from autophagolysosomes (APLys, red) since fusion with acidic lysosomes leads to loss of GFP fluorescence at low pH and unmasking of the mCherry fluorescence (40). Consequently, we infected human iPSC-derived MNs with lentiviruses expressing this construct and analyzed the presence of APs (yellow) and APLys (red) by confocal microscopy. SMA MN cultures displayed an increased number of APs under basal conditions (Figure 4D-E) and a reduced increase in the percentage of APLys upon autophagy induction with rapamycin when compared to wildtype MN cultures (Figure 4D,F), suggesting that formation of APs is not impaired in SMA MNs, but rather their clearance.

We next questioned whether the defect in autophagy activity detected in SMA cells was an indirect consequence of long-term SMN deficiency or whether, by contrast, acute reduction in SMN levels *per se* could lead to autophagy impairment. To answer this question and since MNs have poor transfection efficiency, we used HEK293T cells to silence *SMN1* with siRNA and determined the levels of p62 and ubiquitination by western blot. We observed that both markers were increased after acute loss of SMN when compared to controls (Figure 4G-H), while p62 mRNA expression levels remained unchanged (Figure 4I) indicating that p62 accumulation was non-transcriptional and occurred in essence from reduced turnover. Finally, to rule out the possibility of a UPS activity dysfunction as responsible for the accumulation of p62 and ubiquitin in SMA MNs, we quantified chymotrypsin-like activity in protein lysates from control and SMA iPSC-derived MNs and observed that at least this activity associated with the proteasome complex was not reduced in diseased cells (Figure 4J). Together, these data indicate that the lack of SMN leads to an impairment of autophagy function that, in turn, results in accumulation of p62/ubiquitinated proteins in MNs and non-MNs. However, autophagy activity is not completely blocked and we postulate that it can still sequester p62-SMN protein complexes for degradation.

SMN deficiency leads to mTORC1 activation.

We next sought to explore how deficiency in SMN protein levels led to the autophagy malfunction that eventually resulted in the build-up of protein aggregates or toxic species (24, 41-43). It has been reported that p62, besides serving as an autophagy cargo adaptor, also mediates mTOR activation by promoting its localization to the lysosomal membrane (44, 45). The protein kinase mTOR is the master regulator of cellular metabolism and growth and is part of two protein complexes, mTORC1 and mTORC2 (46). When active, mTORC1 suppresses autophagy at different levels (47-49). Given the accumulation of p62 that we and others have observed in SMA cells (50, 51) and the associated autophagy activity dysfunction, we sought to determine whether decreased SMN levels impacts mTOR activity. To address this question, we compared healthy control human fibroblasts to fibroblasts from patients affected by the most severe forms of the disease, SMA type I and type 0, this last type carrying only 1 *SMN2* copy. We deprived them of serum overnight and then incubated them with full media for 30 minutes to measure mTOR activity. We observed that not only did control-treated SMA fibroblasts show increased phosphorylated levels of the mTOR downstream targets S6K1 and S6 when compared to healthy fibroblasts (Figure 5A and S4A), but also that the decrease in their phosphorylation upon starvation was less pronounced than in control cells, suggesting a higher basal mTOR activity in the diseased fibroblasts. Next, we investigated whether mTOR activity was also enhanced in SMA mouse and human MNs of different severities and obtained similar results, higher levels of p-S6K1 and p-S6 compared to healthy controls (Figure 5B, S4B and Figure 5C-D, respectively). These data indicate that SMN deficiency results in mTOR pathway activation. It has been previously reported that p62 activates mTOR (44, 45). We postulate that these results, together with the elevated p62 observed in SMA affected cells, suggest that the increase in mTORC1 activity in SMA leads to accumulation of p62 protein, which, in turn, activates mTOR resulting in a feed-forward cycle that leads to further autophagy dysfunction and SMN sequestration (Figure 5E).

Reducing p62 levels promotes MN survival *in vitro* and increases the lifespan of fly and mouse SMA models.

Our data show that reducing p62 protein levels leads to notable increases in SMN and other proteins of the SMN complex including gemin2. Consequently, we explored whether this stabilization of SMN and its binding partners is associated with cytoprotection of SMA cells. We

have previously shown that higher SMN levels directly correlate with better survival of both wildtype and SMA MNs under any kind of stress (34, 35). Thus, we decided to investigate the effect on MN survival of a p62-mediated increase in SMN. We knocked-down p62 by lentiviral infection in mouse SMA MNs and quantified the number of surviving Hb9:GFP$^+$ MNs 10 days later. p62 knock-down resulted in a 50% increase in MN survival compared to cultures infected with scramble control virus (NS) (Figure 6 A,B). In addition, p62 knocked-down SMA MNs showed a larger soma size, an indication of better overall neuronal health (Figure 6C). We also explored whether reducing p62 levels in wildtype MNs could reduce the basal rates of death due to culture-intrinsic stress. Indeed, we observed that wildtype MNs also displayed higher survival and larger soma size when p62 was knocked-down when compared to the NS-treated ones (Figure S5A-C).

These results prompted us to investigate whether reducing p62 levels caused an amelioration of the SMA disease phenotype *in vivo*. We first studied a fly model of SMA where the expression of an RNAi targeting Smn is activated only in adult flies using a ubiquitous Tubulin-Gal4 driver which is under control of temperature-sensitive GAL80 protein (Gal80ts). Larvae were raised at 18ºC, when Tubulin-Gal4 is inactive, to prevent SMN reduction from having developmental effects, and adult flies were then switched to 29.5 ºC to drive expression of the RNAi. We used the Actin Gene-Switch (Actin-GS) inducible Gal4/UAS expression system (52, 53), where UAS-RNAi expression is driven by Gal4 when flies are fed mifepristone (RU486). As expected, RNAi against a control gene (w) did not affect lifespan (Figure S6A-B) and Smn RNAi (Smn-i) decreased Smn mRNA levels by 70% (Figure S6A). We did not expect that Smn RNAi would produce a strong decrease in lifespan, given that its expression is only activated during adult life. Indeed, we observed a small, although significant, reduction of the mean lifespan when it was co-expressed with control RNAi (Figure S6A, C). Next, we analyzed the effects of reducing p62 expression on SMN protein levels and observed that it resulted in enhanced SMN protein (Figure S6D-E) without affecting *Smn* mRNA expression (Figure S6F). In addition, we tested whether p62 down-regulation affected the lifespan of *Smn*-deficient flies by co-expressing *Smn*-i with *p62*-i. Importantly, while reducing p62 levels alone did not affect lifespan (Figure S6G-H), flies expressing *Smn*-i and *p62*-i showed a complete rescue of the *Smn* RNAi-induced shortened lifespan (Figure S6I-J). These results indicate that decreasing p62 levels increases SMN protein *in vivo* and rescues the shortened lifespan of SMN-deficient flies.

We next sought to explore whether these observations could be reproduced in the SMA SMNΔ7 mouse, which in our colony survives an average of 10 days. Given than p62 KO mice are fertile and relatively healthy until they reach a mature age, when they develop obesity and bone and metabolic problems (54), we aimed to measure the disease manifestations in p62 KO SMNΔ7 mice. However, breeding SMNΔ7;p62 KO mice resulted in embryonic lethality of SMNΔ7 pups (data not shown), presumably because p62 is a scaffold protein with multiple modules that interact with other key signaling proteins (55). Instead, we crossed SMNΔ7 mice with p62 KO mice in order to obtain SMNΔ7 p62 heterozygote mice (*smn*-/-;h*SMN2*+/+;h*SMN*Δ7+/+;Hb9:GFP+;p62+/- or just SMNΔ7;p62+/- for simplicity). We confirmed that p62 protein levels in spinal cords from SMNΔ7;p62+/- mice were indeed reduced by half (Figure 6D) and then studied several aspects of the mouse SMA disease phenotype. We first used an unbiased, automated method to measure muscle fiber size of tibialis anterior (TA) muscle cryosections at the disease end stage (P10). We observed that SMNΔ7;p62+/- TA muscle fibers showed a significant increase in size compared to SMNΔ7 mice (homozygous for p62) (Figure 6E-F). Next, we evaluated the innervation status of the flexor digitorum brevis-2 (FDB-2) appendicular muscle, which is reported to display strong denervation in SMNΔ7 mice (56). Fully innervated endplates were defined by the complete overlap of presynaptic nerve terminals, immunostained with synaptophysin, and postsynaptic motor endplate acetylcholine receptors labeled with α-bungarotoxin. Partially denervated endplates were identified by the partial overlap of pre- and post-synaptic labeling and fully denervated endplates were devoid of any presynaptic labeling (Figure S5D). The quantification of the percentage of denervated endplates revealed a robust amelioration of this pathologic phenotype in SMNΔ7;p62 mice. While in SMNΔ7 at P10 only 40% of the endplates are fully innervated (Figure 6G-H), in SMNΔ7;p62 mice almost 80% of them were fully innervated and only about 5% were denervated (Figure 6G-H). Additionally, we analyzed the spinal MN loss characteristically seen in this SMA mouse model (30) and observed that while SMNΔ7 mice at P10 displayed a 50% reduction in motor neuron number, SMNΔ7;p62+/- P10 mice showed a similar number of ventral MNs compared to wildtype mice (Figure 6I-J). This notable improvement in muscle, MNs and muscle innervation, correlated with a significant increase in the body weight of SMNΔ7;p62+/- compared to SMNΔ7 mice (Figure 6K). Importantly, the rescue of multiple SMA-associated phenotypes translated to a 50% increase in the mean lifespan (5 more days) (Figure 6L).These data validate our *in vitro* results

and confirm that p62 plays an important role in SMA pathology. Additionally, this work shows that reducing p62 levels, aberrantly increased in the disease, could represent a new strategy to find SMA therapeutics.

Discussion

In this study, we have identified the autophagy receptor p62 as a novel regulator of SMN protein levels and discovered a molecular mechanism that explains the autophagy dysfunction affecting SMA cells. Our data reveals that an mTOR over-activation causes such a dysfunction in SMA MNs, resulting in accumulation of ubiquitinated proteins and p62. We suggest that abnormally high p62 levels aggravate the autophagy impairment and constitute the basis for the build-up of toxic species enhancing susceptibility to cell death.

SMA is an early-onset neuromuscular disease associated with loss of function mutations or complete loss of the *SMN1* gene, resulting in very low SMN protein levels. Therefore, it is commonly accepted that approaches aimed at increasing SMN levels will have therapeutic value in treating the disease. Several of these approaches have recently entered clinical trials after showing promising results in *in vitro* and *in vivo* models (57), with one, Spinraza having been recently approved. However, most of them focus on modifying the expression or the splicing of the *SMN2* gene, or on directly replacing *SMN1* gene via viral delivery. SMN is also controlled at the post-transcriptional level, but to date the approaches addressed at targeting this aspect of SMN biology have not reached therapeutic success. Therefore, one main focus of our work has been to identify new pathways that mediate SMN protein degradation with a view towards stabilizing the protein increasing its levels. It is known that SMN forms part of protein complexes (gems, SG, complexes along axons) whose disassembly and degradation mechanisms are unclear. Since the UPS system, previously shown to regulate SMN levels, only targets single proteins, we focused on the other major cellular catabolic pathway, the autophagy-lysosomal system, in charge of degrading protein complexes, protein aggregates and organelles. We postulated that autophagy could be also regulating SMN protein levels by at least targeting the fraction that is localized to protein complexes. With this study, we found that indeed autophagy degrades SMN, not only SMN-FL, but also the most abundantly transcribed form of SMN in SMA patients, SMN-Δ7, which is partially functional and therefore blocking its degradation may be quite relevant for slowing disease progression.

Our data also show that the autophagy receptor p62 is a mediator of selective SMN degradation. SMN and p62 interact, and this interaction is partially blocked when SMN ubiquitination is inhibited. We also demonstrate that reducing p62 levels leads to a significant enhancement not only of SMN, but also of some of its main binding partners, such as gemin2 and the number of SMN^+, $gemin2^+$ nuclear gems. Importantly, such increases have functional consequences, since they improve survival of SMA MNs *in vitro*, abolished the shortening effect on fly lifespan induced by Smni and notably improved multiple aspects of the disease pathology of SMNΔ7 mice, including increasing their lifespan by 50%.

One recently published study also implicated autophagy in controlling SMN protein levels (51). This work, however, showed that inducing autophagy increases SMN levels while at the same time claimed that SMA cells exhibit increased autophagy. Although, there are differences between our studies, both of them demonstrated the critical role of autophagy in SMA pathogenesis, and our study, using multiple cell types and models, further uncovers the mechanistic control of SMN degradation by selective autophagy via the molecular adaptor p62. Additional studies will be required to understand the discrepancies between our findings and the previously published results.

For many years autophagy was considered to be a bulk-degradation process induced by nutrient deprivation and lacking specificity. However, almost twenty years ago, selective autophagy was reported in yeast (58) and since then, multiple studies have confirmed that autophagy is a more selective process than originally anticipated (59). Indeed, p62 and other proteins with similar amino acid domains, such as NBR1, optineurin, NDP52 and others, have been shown to function as autophagy cargo recognition proteins (31, 32). A hallmark of most neurodegenerative diseases is the accumulation of misfolded and aggregation-prone proteins and damaged organelles (39, 60). Numerous studies have reported the importance of autophagy receptors in delivering protein aggregates and organelles to APs for degradation (22). To date, the presence of these toxic species in SMA had not been reported. However, recent studies have demonstrated intracellular trafficking problems affecting mitochondria (61), the endosomal-lysosomal system (62, 63) and axonal transport, growth or morphology (26, 64-66). An impairment of the last steps of the autophagic process could well be another consequence of a SMN deficiency, but such an autophagy dysfunction could also be the source of those cellular defects, similar to what has been reported for other neurological disorders. These studies together

with the data presented in this work suggest that SMA shares more neurodegenerative diseases hallmarks than previously recognized.

Since autophagy, through p62, plays a role in mediating SMN degradation, and since most neurodegenerative disorders involve defects in autophagy activity, we investigated whether this pathway was functioning properly in SMA. Indeed we have observed that all SMA cells analyzed –human fibroblasts, mouse and human iPSC-derived MNs– display higher amounts of LC3-I and II, which correlates with increased number of APs and impaired AP turnover (Figure 4). We have observed that this defect is accompanied by increased levels of p62 and ubiquitinated proteins and that an acute decrease of SMN protein levels leads to the same results. Our findings agree with recently reported studies that suggest autophagy alterations upon SMN-downregulation in cell lines (50, 67, 68) and explain the previously unresolved questions of why autophagy is dysfunctional in SMA and the nature of the interplay between SMN and autophagy activity. We postulate that, as a consequence of SMN deficiency-induced autophagy impairment, ubiquitinated proteins and p62 accumulate. This is likely to increase the appearance of misfolded and aggregated proteins, leading to additional problems in cellular trafficking and AP clearance. This hypothesis is in line with a previous study from Komatsu and colleagues that demonstrated that p62 plays an important role in inclusion body formation when autophagy is deficient (69). Another possible consequence of enhanced p62 protein levels is over-activation of mTORC1, with would, in turn, further interfere with autophagy activity (70, 71). There is also some disagreement as to the role that mTOR plays in SMA. On the one hand, several studies in SMA mice suggest that mTOR is downregulated and that increasing its activity can promote MN survival and enhance lifespan (72-74). On the other hand, another study showed that SMA type III muscle shows over-expression of mTOR (75). It is therefore possible that the activity of mTOR in SMA differs between different tissues or even cell populations. The increased mTOR activity that we detect in SMA cells could be a cellular response to limit further accumulation of APs and aggregation-prone material, but at the same time it could be blocking autophagy reactivation via its inhibitory effect on TFEB, the master transcriptional regulator of lysosomal and autophagy genes (76, 77). Further studies are needed to unravel whether the observed alterations on the autophagy/lysosomal function and mTORC1 signaling pathway in SMA MNs are direct, and maybe independent, consequences of SMN loss of function, or the indirect result of accumulative events triggered by the deficiency of the protein.

In summary, in this study, we have identified a new pathway that controls SMN levels in cells including MNs, which can uncover new avenues for finding potential targets for therapeutic intervention. Furthermore, we have revealed an autophagy dysfunction in SMA MNs possibly caused by mTOR over-activation, resulting in accumulation of ubiquitinated proteins and p62. p62 is a key protein which links autophagy, mTORC1, ubiquitination and, now, SMN protein levels. We postulate that abnormally high p62 levels may aggravate autophagy impairment and constitute the basis for the build-up of toxic species enhancing susceptibility to cell death. Understanding the molecular mechanisms that control this loop, as well as whether compromised autophagy contributes to SMA progression, will be essential for future development of therapeutics that act on this pathway to prevent neuronal degeneration.

Materials and Methods

Study approval. All animal studies were reviewed and approved by Harvard University Institutional Animal Care and Use Committee (Cambridge, MA) and performed in accordance with institutional and federal guidelines. The Pediatric Neuromuscular Clinical Research Network recruited SMA patients and collected the fibroblasts later obtained by the Rubin lab for the derivation of iPS cell lines. Tissue collections for all human subjects that donated tissue used in this research were conducted with consent under protocols that were approved by the Columbia University IRB (New York, NY). Subsequent use of the SMA patient samples in the Rubin lab at Harvard University was reviewed by the Harvard University Committee on the Use of Human Subjects (CUHS) (Cambridge, MA). Generation of iPSC lines by the Harvard iPSC Core was conducted in a fee-for-service capacity. The information regarding both the SMA iPSC lines and the healthy control lines BJ and 1016A is enclosed in Rodriguez-Muela *et al* 2017(35).

Mouse colonies. FVB mice were obtained from Charles River Laboratories. The original breeding pair of heterozygous SMNΔ7 mice (*Smn*+/–;h*SMN2*+/+;h*SMNΔ7*+/+) on a FVB background, and the *Hb9:GFP* mice on a C57Bl/6/ background, were provided by the Jackson Laboratory and back-crossed to a FVB background for more than 10 generations. *p62/SQSTM1*-/- mice on a C57Bl/6/ background were kindly provided by Dr. Toru Yanagawa (University of Tsukuba, Tsukuba, Japan) and back-crossed to a FVB background for more than 7 generations.

Spinal MN and muscle histology. The spinal cord and tibialis anterior (TA) muscles were dissected from wildtype, SMNΔ7 and SMNΔ7;p62+/- mice euthanized at postnatal day 10 and fixed in 4% paraformaldehyde in PBS overnight (o/n). The spinal corsd were processed as previously described (35) and images were captured with LSM 700 Inverted Confocal (Leica). For evaluating the innervation state of the flexor digitorum brevis 2 (FDB-2) muscle hind paws were fixed in 4% paraformaldehyde in PBS o/n and then rinsed in PBS. The FDB-2 muscles were dissected, permeabilized in 0.5% Triton-X100 and blocked in 5% NGS under constant shaking for 1 hour, then incubated with anti-synaptophysin antibody for 24 hours at 4C. Samples were subsequently washed with several changes of PBS shaking for 6 hours, incubated with secondary antibody o/n at 4C and then washed with PBS shaking for 6 hours. Finally, samples were incubated with α-bungarotoxin for 1 hour at room temperature to label AChRs, washed again for 1 hour and mounted and imaged as described above.

Mouse MN Differentiation. Mouse wildtype SMN+/+;SMN2+/+;Hb9:GFP and SMA SMN-/-;SMN2+/+;Hb9:GFP, and SMN-/-;SMN2+/+;SMNΔ7;Hb9:GFP ES cells were maintained and differentiated as described previously (35). Briefly, ES cells were differentiated into MNs using an embryoid body method with treatments of retinoic acid (Sigma-Aldrich), and a hedgehog agonist (Curis Inc.). After 7 days, MNs were dissociated and plated onto poly-ornithine coated plates (PerkinElmer).

Human MN Differentiation. The iPSC were grown on Matrigel-coated dishes (BD Biosciences), cultured with mTeSR (StemCell Technologies) and split using Gentle Cell Dissociation Reagent (StemCell Technologies) until the initiation of the MN differentiation protocol, when they were dissociated with Accutase (StemCell Technologies) and cultured in mTeSR as embryoid bodies in ultra-low attachment dishes (Corning). 1 µM LDN (Stemgent) and 10 µM SB 431542 (Stemgent) were added one day later (day 1) to induce neural differentiation and media gradually changed to knockout serum replacement/DMEM media (Life Technologies). 1 µM retinoic acid (Sigma-Aldrich) and 10 ng/mL BDNF were added two days later (day 3) and 1 µM smoothened agonist 1.3 (EMD Millipore) was added 5 days later (day 8). 2.5 µM DAPT (R&D Systems) was added at day 10 along with, 2 µM Cytosine Arabinoside (Ara-c, Sigma-Aldrich) to eliminate progenitors and dividing cells. From day 5 to day 10 media

was gradually changed to DMEM/F12 supplemented with 2% B27 and 1% N2 (Life Technologies). After 14 days of differentiation the cultures were dissociated with papain/DNase solution (Worthington) and plated in 50µg/ml poly-lysin (EMD Millipore), 10µg/ml laminin (Life Technologies) and 10µg/ml fibronectin (Corning) coated plates (Greiner). The medium used was Neurobasal containing 2% B27 and 1% N2, supplemented with Glutamax (Life Technologies), NEAA (EMD Millipore), 20% glucose, 0.2µM ascorbic acid (Sigma) and 20 ng/ml of BDNF, GDNF, and CNTF (R&D Systems).

Immunocytochemistry and Image Analysis. Cells were fixed in 4% paraformaldehyde (PFA) at room temperature for 20 min. Following standard protocols, cells were immunostained with the indicated primary antibodies followed by fluorescently labeled secondary antibodies (Life Technologies) as previously described (35). For quantification of mCherry-LC3$^+$ APLys and mCherry-GFP-LC3$^+$ APs, human iPSC-derived MNs were cultured in 12mm glass coverslips and images captured with a 63X objective in a LSM 700 Inverted Confocal Microscope (Leica). Quantifications were performed on images with maximum projection of all Z-stack sections using ImageJ software (NIH) from 40-100 lentiviral-transduced neurons per line and per treatment. Three independent experiments were performed. TA muscle fiber size was quantified on images taken with a 20X objective in a Nikon Eclipse Ti microscope from random visual fields. Subsequent image quantification was automatically performed using the Columbus Image Data Storage and Analysis System. 2000-3000 muscle fibers per mouse were measured. Innervation of FDB-2 muscles was quantified on images taken with a 20X objective in a LSM 700 Inverted Confocal Microscope. The innervation status of postsynaptic endplates was determined according to the extent to which the endplate overlaid with presynaptic components. Fully innervated endplates were defined by the complete overlap of presynaptic (i.e. synaptophysin) and postsynaptic (α-bungarotoxin) labeling. Partially denervated endplates were identified as only part of the endplate being covered by presynaptic labeling. Fully denervated endplates were devoid of any presynaptic labeling. 300-700 endplates per mouse were analyzed from randomly selected visual fields. The quantification was performed blinded to the genotypes of muscles.

Chemicals, Antibodies, and Plasmids. For mammalian cell experiments, antibodies for rat HA and mouse β-actin (Cell Signaling Technology, 3700S), rabbit beta-tubulin (ab6046), rabbit Islet1 (ab109517), SQSTM1/p62 (ab56416), rabbit Gemin2 (ab150383) rabbit and Lamin B1 (ab16048) (Abcam), mouse SMN (BD Biosciences, 610647), rabbit Ubiquitin (Santa Cruz Biotechnology, SC-9133), mouse c-Myc (Novus Biologicals, NB600-302), rabbit LC3 (2775), rabbit p-P70S6K1 (Thr389, 9234S), rabbit P70S6K1 (2708S), rabbit p-S6 (Ser235/236, 2211s), rabbit S6 (2217S) (Cell Signaling Technology), synaptophysin (Synaptic Systems, 101002) and laminin (Sigma Aldrich, L9393) were used as indicated. For NMJ analysis Alexa Fluor 555-conjugated α-bungarotoxin (Life Technologies, B35451) was used. For fly experiments, SMN (gift from Dr. Spyros Artavanis-Tsakonas, Harvard Medical School, Boston, MA and Dr. Gregory Matera (University of North Carolina, Chapel Hill, NC) and tubulin (Sigma-Aldrich, T5168) antibodies were used. cDNAs encoding human HA-tagged full-length SMN (FL) protein or a truncated SMN protein carrying a deletion of exon 7 (Δ7) were cloned into the pEF-DEST51 vector using the Gateway cloning system (Life Technologies). Myc-p62 plasmid was kindly provided by Dr. María T. Diaz-Meco (Sanford Burnham Prebys Medical Discovery Institute, La Jolla, CA) and HA-GFP and myc-E2-crimson plasmids were purchased from Addgene (22612 and 38770 respectively).

Transfection and lentiviral transduction. For overexpression of SMN-FL and SMN-Δ7 proteins, HEK293T cells were transfected with Lipofectamine 2000 (Life Technologies) with the HA-tagged forms of the proteins following manufacturer´s instructions. 20 nM of a pool of RNAi against p62/SQSTM1 or SMN was transfected in HEK293T (Santa Cruz Biotechnology, sc-29679 and sc-36510, respectively) and mouse MNs (Santa Cruz Biotechnology, sc-29828) or control RNAi (Qiagen 1027280) using Lipofectamine RNAiMAX Transfection Reagent (Life Technologies) following manufacturer´s instructions. Cells were exposed to the silencing mix for 6 hours following which silencing medium was replaced with fresh complete media. Lentiviral shRNA plasmids targeting Atg7 and a non-silencing control, as well as mCh-GFP-LC3 constructs were kindly provided by Dr. Ana M. Cuervo (Albert Einstein College of Medicine, New York, NY) and previously published. Plasmids encoding the dominant negative form of human Cullin5 in PHAGE vector and empty PHAGE vector were purchased from Addgene (41916 and 44012 respectively) and used for lentiviral production. Vectors encoding short

hairpins against mouse (TRCN0000238133 and TRCN0000098615) and human (TRCN0000430110 and TRCN0000007234) p62/SQSTM1 were purchased from Sigma-Aldrich. Lentiviral stocks were prepared by lipofectamine transfection of these vectors and the packaging vectors pMDLg/pRRE, pRSV-Rev and pMD2.VSVG into HEK293T cells. Supernatants were collected over 72 hours, titred and used for infection. The efficiency of infection at 72 hours, determined by the percent of GFP+ cells or the percent of cells surviving 1µM puromycin treatment, depending on the vector, exceeded 90% for all constructs.

Cell culture treatments. For serum or amino acid removal, cells were washed with phosphate-buffered saline (PBS) followed by culture in DMEM or EBSS for 24 hours, respectively, where indicated. Lysosomal inhibitors, leupeptin (Fisher BioReagents), ammonium chloride (Sigma-Aldrich) and hydroxychloroquine (Sigma-Aldrich) were used at 100µM, 20mM and 10µM, respectively, for 4-6 hours. Rapamycin (R & D Systems) was used at 200 nM, and MG132 (Sigma-Aldrich) at 100 nM for the indicated times. For stress granule formation induction, cells were exposed to 10 or 50 µM sodium arsenate for 6h. Details for immunoprecipitation, cellular fractionation and immunoblot analysis are specified in Supplemental Experimental Procedures.

Chymotrypsin-like activity measurement. Human iPSC-derived MNs were washed in PBS, homogenized with 0.5% NP-40 and centrifuged for 15 min at 4°C at 13.000 rpm. Supernatant were collected and the assay performed following manufacturer´s instructions (Proteasome Activity Assay Kit (Abcam, ab107921).

Reverse Transcription-PCR. Total RNA was extracted with the TRIzol reagent (Life Technologies), followed by DNase digestion using RQ1 RNase-Free DNase (Promega). Total RNA was reverse transcribed with the iScript cDNA synthesis kit (Bio-Rad). qRT-PCR was performed with the iQ SYBR Green Supermix (Bio-Rad) and a CFX96 Real-Time PCR Detection System (Bio-Rad). Relative quantitations of mRNA levels were determined with the comparative CT method. For mammalian cell experiments, 18s and actin were used as house-keeping genes, and for fly experiments RpL32 and alpha-Tubulin 84B were used as a normalization reference. Mouse primers used: SMN F: aaggcacagccagaagaaaa, SMN R: tcacaggtcggggaaagtag; p62 F: gctgccctatacccacatct, p62 R: cgccttcatccgagaaac; IL6 F: agttgccttcttgggactga, IL6 R: tccacgatttcccagagaac. Human primers used: SMN F:

aacatcaagcccaaatctgc, SMN R: tggtccagaaggaaatggag; p62 F: agaacgttggggagagtgtg, p62 R: gcgatcttcctcatctgctc. Primers used for fly: Smn F: agcggaaagaaaaagacacc; Smn R: tcgaaaagatgtgatgtgatga; ref(2)P(p62) F: aatcgagctgtatcttttccagg; ref(2)P (p62) R: aacgtgcatattgctctcgca.

Fly Lifespan analysis. For survival analysis, flies were collected within 24 hrs from eclosion, sorted by sex under light CO2 anesthesia, and reared at standard density (20-25 flies per vial) on cornmeal/soy flour/yeast fly food at 25°C and 60% humidity with 12 hrs on/off light cycle. Flies were transferred to fresh vials every two days and dead flies counted. RU486 (Mifepristone) dissolved in ethanol was administered in the media at the final concentration of 150 µg/mL. Efficiency of Smn and p62 RNAi lines was tested using the ubiquitous Actin5c-Gal4 driver. As control we used RNAi against *white* gene, responsible for the eye color that we and others have showed does not affect lifespan when it is mutated or suppressed with RNAi (78). The following RNAi lines were used: Control RNAi (HMS00017), Smn-i (JF02057); p62-551i (HMS00551) and p62-938i (HMS00938).

Statistical Analysis. Statistical significance was determined by Two-tailed Student's *t*-test for groups of two and by analysis of variance (ANOVA) for groups of 3 or more. A confidence interval of 95% was used for all comparisons. The statistical significance for the Kaplan-Meier analysis was determined by Mantel-Cox and Wilcoxon tests. A "*p* value" less than 0.05 was considered significant. $*p< 0.05$, $**p< 0.01$, $***p< 0.001$.

Acknowledgements

We thank the Pediatric Neuromuscular Clinical Research Network for recruiting SMA patients and the Harvard iPSC Core for generating the iPSC from SMA patient fibroblasts. We thank Catherine McGillivary and Diane Faria for histology assistance. We thank Dr. Patricia Boya for critically reviewing this manuscript. We are grateful to Lance S. Davidow for image analysis support and to J. LaLonde for editorial assistance. The work was supported by the Muscular Dystrophy Association -MDA376743- (NRM), SMA Foundation (LLR), National Institute of Neurological Disorders and Stroke -P01NS066888- (LLR), National Institute of General Medical

Sciences -R01-AG043517 (RS) and R01-GM084947 (NP)-. A.P. is supported by The LAM Foundation Fellowship Award (LAM00105E01-15).

Author contributions.

Conceptualization, N.R-M. and A.P.; Methodology, N.R-M, A.P. and T.G.; Formal Analysis, N.R-M and A.P.; Investigation, N.R-M, A.P., RM.G. and T.G.; Research assistance, E.M.N.; Resources, N.R-M, A.P., N.P. and L.L.R.; Writing Original Draft, N.R-M; Review and Editing, N.R-M, A.P., T.G., N.P., R.S. and L.L.R.; Funding Acquisition, N.R-M and L.L.R.

References

1. Lefebvre S, Burglen L, Reboullet S, Clermont O, Burlet P, Viollet L, et al. Identification and characterization of a spinal muscular atrophy-determining gene. *Cell.* 1995;80(1):155-65.
2. Iascone DM, Henderson CE, and Lee JC. Spinal muscular atrophy: from tissue specificity to therapeutic strategies. *F1000prime reports.* 2015;7:04.
3. Lorson CL, Hahnen E, Androphy EJ, and Wirth B. A single nucleotide in the SMN gene regulates splicing and is responsible for spinal muscular atrophy. *Proc Natl Acad Sci U S A.* 1999;96(11):6307-11.
4. Monani UR, Lorson CL, Parsons DW, Prior TW, Androphy EJ, Burghes AH, et al. A single nucleotide difference that alters splicing patterns distinguishes the SMA gene SMN1 from the copy gene SMN2. *Hum Mol Genet.* 1999;8(7):1177-83.
5. Lorson CL, Strasswimmer J, Yao JM, Baleja JD, Hahnen E, Wirth B, et al. SMN oligomerization defect correlates with spinal muscular atrophy severity. *Nat Genet.* 1998;19(1):63-6.
6. Cho SC, and Dreyfuss G. A degron created by SMN2 exon 7 skipping is a principal contributor to spinal muscular atrophy severity. *Genes Dev.* 2010;24(5):438-42.
7. Gubitz AK, Feng W, and Dreyfuss G. The SMN complex. *Exp Cell Res.* 2004;296(1):51-6.
8. Fallini C, Rouanet JP, Donlin-Asp PG, Guo P, Zhang H, Singer RH, et al. Dynamics of survival of motor neuron (SMN) protein interaction with the mRNA-binding protein IMP1 facilitates its trafficking into motor neuron axons. *Developmental neurobiology.* 2014;74(3):319-32.
9. Lim SR, and Hertel KJ. Modulation of survival motor neuron pre-mRNA splicing by inhibition of alternative 3' splice site pairing. *J Biol Chem.* 2001;276(48):45476-83.
10. Hua Y, Vickers TA, Okunola HL, Bennett CF, and Krainer AR. Antisense masking of an hnRNP A1/A2 intronic splicing silencer corrects SMN2 splicing in transgenic mice. *Am J Hum Genet.* 2008;82(4):834-48.
11. Williams JH, Schray RC, Patterson CA, Ayitey SO, Tallent MK, and Lutz GJ. Oligonucleotide-mediated survival of motor neuron protein expression in CNS improves phenotype in a mouse model of spinal muscular atrophy. *J Neurosci.* 2009;29(24):7633-8.
12. Osman EY, Miller MR, Robbins KL, Lombardi AM, Atkinson AK, Brehm AJ, et al. Morpholino antisense oligonucleotides targeting intronic repressor Element1 improve phenotype in SMA mouse models. *Hum Mol Genet.* 2014;23(18):4832-45.
13. Dickson A, Osman E, and Lorson CL. A negatively acting bifunctional RNA increases survival motor neuron both in vitro and in vivo. *Human gene therapy.* 2008;19(11):1307-15.
14. Naryshkin NA, Weetall M, Dakka A, Narasimhan J, Zhao X, Feng Z, et al. Motor neuron disease. SMN2 splicing modifiers improve motor function and longevity in mice with spinal muscular atrophy. *Science.* 2014;345(6197):688-93.
15. Kwon DY, Motley WW, Fischbeck KH, and Burnett BG. Increasing expression and decreasing degradation of SMN ameliorate the spinal muscular atrophy phenotype in mice. *Hum Mol Genet.* 2011;20(18):3667-77.
16. Burnett BG, Munoz E, Tandon A, Kwon DY, Sumner CJ, and Fischbeck KH. Regulation of SMN protein stability. *Mol Cell Biol.* 2009;29(5):1107-15.
17. Makhortova NR, Hayhurst M, Cerqueira A, Sinor-Anderson AD, Zhao WN, Heiser PW, et al. A screen for regulators of survival of motor neuron protein levels. *Nat Chem Biol.* 2011;7(8):544-52.

18. Kwon DY, Dimitriadi M, Terzic B, Cable C, Hart AC, Chitnis A, et al. The E3 ubiquitin ligase mind bomb 1 ubiquitinates and promotes the degradation of survival of motor neuron protein. *Mol Biol Cell.* 2013;24(12):1863-71.
19. Han KJ, Foster DG, Zhang NY, Kanisha K, Dzieciatkowska M, Sclafani RA, et al. Ubiquitin-specific protease 9x deubiquitinates and stabilizes the spinal muscular atrophy protein-survival motor neuron. *J Biol Chem.* 2012;287(52):43741-52.
20. Xu C, Kim NG, and Gumbiner BM. Regulation of protein stability by GSK3 mediated phosphorylation. *Cell Cycle.* 2009;8(24):4032-9.
21. Mizushima N, and Komatsu M. Autophagy: renovation of cells and tissues. *Cell.* 2011;147(4):728-41.
22. Xu Z, Yang L, Xu S, Zhang Z, and Cao Y. The receptor proteins: pivotal roles in selective autophagy. *Acta biochimica et biophysica Sinica.* 2015;47(8):571-80.
23. Zaffagnini G, and Martens S. Mechanisms of Selective Autophagy. *J Mol Biol.* 2016;428(9 Pt A):1714-24.
24. Hara T, Nakamura K, Matsui M, Yamamoto A, Nakahara Y, Suzuki-Migishima R, et al. Suppression of basal autophagy in neural cells causes neurodegenerative disease in mice. *Nature.* 2006;441(7095):885-9.
25. Pickford F, Masliah E, Britschgi M, Lucin K, Narasimhan R, Jaeger PA, et al. The autophagy-related protein beclin 1 shows reduced expression in early Alzheimer disease and regulates amyloid beta accumulation in mice. *J Clin Invest.* 2008;118(6):2190-9.
26. Komatsu M, Wang QJ, Holstein GR, Friedrich VL, Jr., Iwata J, Kominami E, et al. Essential role for autophagy protein Atg7 in the maintenance of axonal homeostasis and the prevention of axonal degeneration. *Proc Natl Acad Sci U S A.* 2007;104(36):14489-94.
27. Fimia G, Stoykova A, Romagnoli A, Giunta L, Di Bartolomeo S, Nardacci R, et al. Ambra1 regulates autophagy and development of the nervous system. *Nature.* 2007;447(7148):1121-5.
28. Liang CC, Wang C, Peng X, Gan B, and Guan JL. Neural-specific deletion of FIP200 leads to cerebellar degeneration caused by increased neuronal death and axon degeneration. *J Biol Chem.* 2010;285(5):3499-509.
29. Protter DS, and Parker R. Principles and Properties of Stress Granules. *Trends Cell Biol.* 2016;26(9):668-79.
30. Le TT, Pham LT, Butchbach ME, Zhang HL, Monani UR, Coovert DD, et al. SMNDelta7, the major product of the centromeric survival motor neuron (SMN2) gene, extends survival in mice with spinal muscular atrophy and associates with full-length SMN. *Hum Mol Genet.* 2005;14(6):845-57.
31. Kirkin V, McEwan DG, Novak I, and Dikic I. A role for ubiquitin in selective autophagy. *Mol Cell.* 2009;34(3):259-69.
32. Slobodkin MR, and Elazar Z. The Atg8 family: multifunctional ubiquitin-like key regulators of autophagy. *Essays in biochemistry.* 2013;55:51-64.
33. Pankiv S, Clausen TH, Lamark T, Brech A, Bruun JA, Outzen H, et al. p62/SQSTM1 binds directly to Atg8/LC3 to facilitate degradation of ubiquitinated protein aggregates by autophagy. *J Biol Chem.* 2007;282(33):24131-45.
34. Ng SY, Soh BS, Rodriguez-Muela N, Hendrickson DG, Price F, Rinn JL, et al. Genome-wide RNA-Seq of Human Motor Neurons Implicates Selective ER Stress Activation in Spinal Muscular Atrophy. *Cell stem cell.* 2015.
35. Rodriguez-Muela N, Litterman NK, Norabuena EM, Mull JL, Galazo MJ, Sun C, et al. Single-Cell Analysis of SMN Reveals Its Broader Role in Neuromuscular Disease. *Cell reports.* 2017;18(6):1484-98.
36. Hua Y, and Zhou J. Survival motor neuron protein facilitates assembly of stress granules. *FEBS Lett.* 2004;572(1-3):69-74.

37. Zou T, Yang X, Pan D, Huang J, Sahin M, and Zhou J. SMN deficiency reduces cellular ability to form stress granules, sensitizing cells to stress. *Cell Mol Neurobiol.* 2011;31(4):541-50.
38. Klionsky DJ, Abdelmohsen K, Abe A, Abedin MJ, Abeliovich H, Acevedo Arozena A, et al. Guidelines for the use and interpretation of assays for monitoring autophagy (3rd edition). *Autophagy.* 2016;12(1):1-222.
39. Frake RA, Ricketts T, Menzies FM, and Rubinsztein DC. Autophagy and neurodegeneration. *J Clin Invest.* 2015;125(1):65-74.
40. Kimura S, Noda T, and Yoshimori T. Dissection of the autophagosome maturation process by a novel reporter protein, tandem fluorescent-tagged LC3. *Autophagy.* 2007;3(5):452-60.
41. Komatsu M, Waguri S, Chiba T, Murata S, Iwata J, Tanida I, et al. Loss of autophagy in the central nervous system causes neurodegeneration in mice. *Nature.* 2006;441(7095):880-4.
42. Boya P, Gonzalez-Polo RA, Casares N, Perfettini J, Dessen P, Larochette N, et al. Inhibition of macroautophagy triggers apoptosis. *Mol Cell Biol.* 2005;25(3):1025-40.
43. Korolchuk VI, Mansilla A, Menzies FM, and Rubinsztein DC. Autophagy inhibition compromises degradation of ubiquitin-proteasome pathway substrates. *Mol Cell.* 2009;33(4):517-27.
44. Duran A, Amanchy R, Linares JF, Joshi J, Abu-Baker S, Porollo A, et al. p62 is a key regulator of nutrient sensing in the mTORC1 pathway. *Mol Cell.* 2011;44(1):134-46.
45. Dibble CC, and Manning BD. Signal integration by mTORC1 coordinates nutrient input with biosynthetic output. *Nat Cell Biol.* 2013;15(6):555-64.
46. Saxton RA, and Sabatini DM. mTOR Signaling in Growth, Metabolism, and Disease. *Cell.* 2017;169(2):361-71.
47. Ganley IG, Lam du H, Wang J, Ding X, Chen S, and Jiang X. ULK1.ATG13.FIP200 complex mediates mTOR signaling and is essential for autophagy. *J Biol Chem.* 2009;284(18):12297-305.
48. Jung CH, Jun CB, Ro SH, Kim YM, Otto NM, Cao J, et al. ULK-Atg13-FIP200 complexes mediate mTOR signaling to the autophagy machinery. *Mol Biol Cell.* 2009;20(7):1992-2003.
49. Kim J, Kundu M, Viollet B, and Guan KL. AMPK and mTOR regulate autophagy through direct phosphorylation of Ulk1. *Nat Cell Biol.* 2011;13(2):132-41.
50. Custer SK, and Androphy EJ. Autophagy dysregulation in cell culture and animals models of spinal muscular atrophy. *Mol Cell Neurosci.* 2014;61:133-40.
51. Periyakaruppiah A, de la Fuente S, Arumugam S, Bahi N, Garcera A, and Soler RM. Autophagy modulators regulate survival motor neuron protein stability in motoneurons. *Exp Neurol.* 2016;283(Pt A):287-97.
52. Osterwalder T, Yoon KS, White BH, and Keshishian H. A conditional tissue-specific transgene expression system using inducible GAL4. *Proc Natl Acad Sci U S A.* 2001;98(22):12596-601.
53. Roman G, Endo K, Zong L, and Davis RL. P[Switch], a system for spatial and temporal control of gene expression in Drosophila melanogaster. *Proc Natl Acad Sci U S A.* 2001;98(22):12602-7.
54. Rodriguez A, Duran A, Selloum M, Champy MF, Diez-Guerra FJ, Flores JM, et al. Mature-onset obesity and insulin resistance in mice deficient in the signaling adapter p62. *Cell Metab.* 2006;3(3):211-22.
55. Katsuragi Y, Ichimura Y, and Komatsu M. p62/SQSTM1 functions as a signaling hub and an autophagy adaptor. *FEBS J.* 2015;282(24):4672-8.
56. Ling KK, Gibbs RM, Feng Z, and Ko CP. Severe neuromuscular denervation of clinically relevant muscles in a mouse model of spinal muscular atrophy. *Hum Mol Genet.* 2012;21(1):185-95.

57. Faravelli I, Nizzardo M, Comi GP, and Corti S. Spinal muscular atrophy--recent therapeutic advances for an old challenge. *Nat Rev Neurol.* 2015;11(6):351-9.
58. Hutchins MU, Veenhuis M, and Klionsky DJ. Peroxisome degradation in Saccharomyces cerevisiae is dependent on machinery of macroautophagy and the Cvt pathway. *J Cell Sci.* 1999;112 (Pt 22):4079-87.
59. Ichimura Y, Kominami E, Tanaka K, and Komatsu M. Selective turnover of p62/A170/SQSTM1 by autophagy. *Autophagy.* 2008;4(8):1063-6.
60. Wong E, and Cuervo AM. Autophagy gone awry in neurodegenerative diseases. *Nat Neurosci.* 2010;13(7):805-11.
61. Miller N, Shi H, Zelikovich AS, and Ma YC. Motor Neuron Mitochondrial Dysfunction in Spinal Muscular Atrophy. *Hum Mol Genet.* 2016.
62. Dimitriadi M, Derdowski A, Kalloo G, Maginnis MS, O'Hern P, Bliska B, et al. Decreased function of survival motor neuron protein impairs endocytic pathways. *Proc Natl Acad Sci U S A.* 2016;113(30):E4377-86.
63. Hosseinibarkooie S, Peters M, Torres-Benito L, Rastetter RH, Hupperich K, Hoffmann A, et al. The Power of Human Protective Modifiers: PLS3 and CORO1C Unravel Impaired Endocytosis in Spinal Muscular Atrophy and Rescue SMA Phenotype. *Am J Hum Genet.* 2016;99(3):647-65.
64. Wang QJ, Ding Y, Kohtz DS, Mizushima N, Cristea IM, Rout MP, et al. Induction of autophagy in axonal dystrophy and degeneration. *J Neurosci.* 2006;26(31):8057-68.
65. Friedman LG, Lachenmayer ML, Wang J, He L, Poulose SM, Komatsu M, et al. Disrupted autophagy leads to dopaminergic axon and dendrite degeneration and promotes presynaptic accumulation of alpha-synuclein and LRRK2 in the brain. *J Neurosci.* 2012;32(22):7585-93.
66. Rodriguez-Muela N, Germain F, Marino G, Fitze PS, and Boya P. Autophagy promotes survival of retinal ganglion cells after optic nerve axotomy in mice. *Cell Death Differ.* 2012;19(1):162-9.
67. Garcera A, Bahi N, Periyakaruppiah A, Arumugam S, and Soler RM. Survival motor neuron protein reduction deregulates autophagy in spinal cord motoneurons in vitro. *Cell Death Dis.* 2013;4:e686.
68. Piras A, Schiaffino L, Boido M, Valsecchi V, Guglielmotto M, De Amicis E, et al. Inhibition of autophagy delays motoneuron degeneration and extends lifespan in a mouse model of spinal muscular atrophy. *Cell Death Dis.* 2017;8(12):3223.
69. Komatsu M, Waguri S, Koike M, Sou YS, Ueno T, Hara T, et al. Homeostatic levels of p62 control cytoplasmic inclusion body formation in autophagy-deficient mice. *Cell.* 2007;131(6):1149-63.
70. Hara K, Maruki Y, Long X, Yoshino K, Oshiro N, Hidayat S, et al. Raptor, a binding partner of target of rapamycin (TOR), mediates TOR action. *Cell.* 2002;110(2):177-89.
71. Linares JF, Duran A, Yajima T, Pasparakis M, Moscat J, and Diaz-Meco MT. K63 polyubiquitination and activation of mTOR by the p62-TRAF6 complex in nutrient-activated cells. *Mol Cell.* 2013;51(3):283-96.
72. Ning K, Drepper C, Valori CF, Ahsan M, Wyles M, Higginbottom A, et al. PTEN depletion rescues axonal growth defect and improves survival in SMN-deficient motor neurons. *Hum Mol Genet.* 2010;19(16):3159-68.
73. Tseng YT, Chen CS, Jong YJ, Chang FR, and Lo YC. Loganin possesses neuroprotective properties, restores SMN protein and activates protein synthesis positive regulator Akt/mTOR in experimental models of spinal muscular atrophy. *Pharmacological research.* 2016;111:58-75.
74. Kye MJ, Niederst ED, Wertz MH, Goncalves Ido C, Akten B, Dover KZ, et al. SMN regulates axonal local translation via miR-183/mTOR pathway. *Hum Mol Genet.* 2014;23(23):6318-31.

75. Millino C, Fanin M, Vettori A, Laveder P, Mostacciuolo ML, Angelini C, et al. Different atrophy-hypertrophy transcription pathways in muscles affected by severe and mild spinal muscular atrophy. *BMC medicine.* 2009;7:14.
76. Sardiello M, Palmieri M, di Ronza A, Medina DL, Valenza M, Gennarino VA, et al. A gene network regulating lysosomal biogenesis and function. *Science.* 2009;325(5939):473-7.
77. Settembre C, Zoncu R, Medina DL, Vetrini F, Erdin S, Huynh T, et al. A lysosome-to-nucleus signalling mechanism senses and regulates the lysosome via mTOR and TFEB. *EMBO J.* 2012;31(5):1095-108.
78. Parkhitko AA, Binari R, Zhang N, Asara JM, Demontis F, and Perrimon N. Tissue-specific down-regulation of S-adenosyl-homocysteine via suppression of dAhcyL1/dAhcyL2 extends health span and life span in Drosophila. *Genes Dev.* 2016;30(12):1409-22.

Figures and Figure Legends

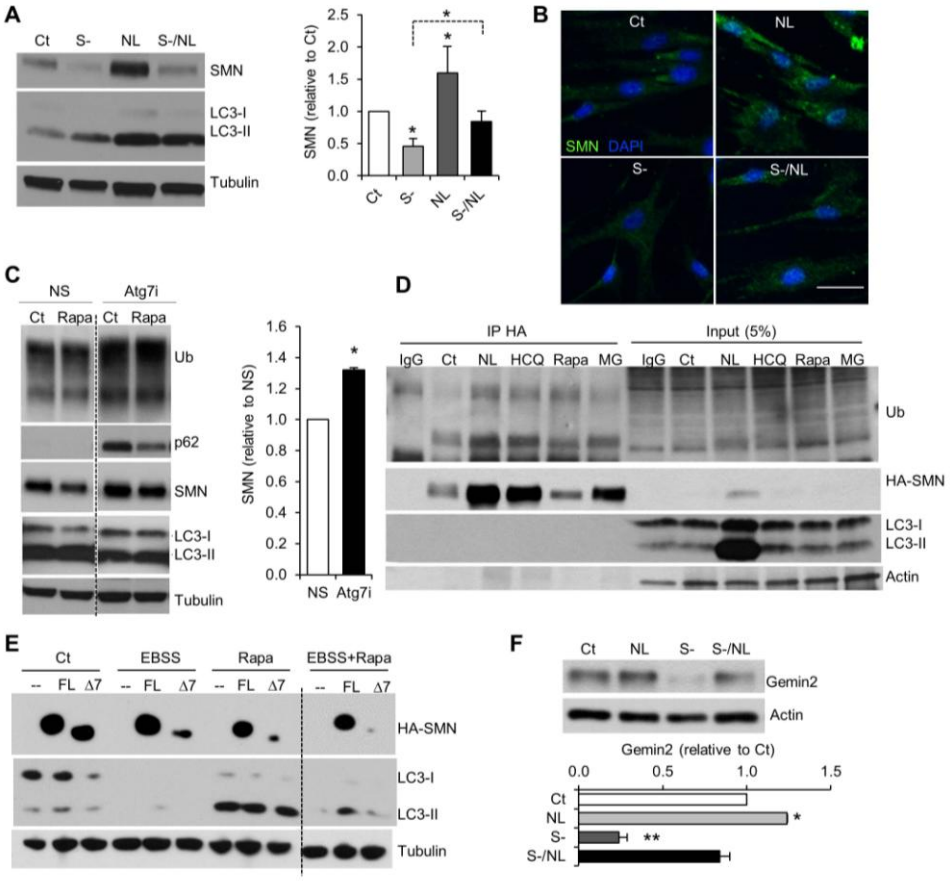

Figure 1. Autophagy regulates SMN protein levels. (**A**) Representative immunoblot and quantification from protein lysates from human control fibroblasts after treatment with lysosomal inhibitors (N/L, ammonium chloride plus leupeptin), serum starvation (S-) or the combination of both (S-, N/L) for 24 hours (Two-tailed t-test, *n*=5 independent experiments). (**B**) Representative image of immunostaining against SMN (green) on human control fibroblasts after the indicated treatments (nuclei labeled with DAPI, blue). Scale bar, 50 µm. (**C**) Representative immunoblot and quantification from protein lysates from wildtype mouse ESC-derived MNs infected with lentivirus carrying shRNA against Atg7 (Atg7i) or empty control (NS, non-silenced) for 7 days and treated the last 24 hours of the culture with rapamycin or control media (Results expressed relative to NS-control cells. Two-tailed *t*-test, *n*=3 independent experiments). (**D**) Representative immunoprecipitation from HEK293T lysates transfected with HA-SMN plasmid and treated with lysosomal inhibitors (NL, combination of ammonium chloride and leupeptin; HCQ, hydroxychloroquine), rapamycin or the proteasome inhibitor MG132 (MG) for 24 hours and immunoblotted against Ubiquitin, HA, LC3 and actin. (**E**) Representative immunoblot from HEK293T lysates transfected with empty vector (--) or the HA-tagged versions of SMN-FL or SMN-Δ7 and cultured in control or aa-free media (EBSS), rapamycin or both for 24 hours. (**F**) Representative immunoblot and quantification from human control fibroblasts after 24 hour treatment with serum free media, NL or both showing the levels of the SMN-binding partner gemin2 (member of the SMN complex) (Two-tailed *t*-test, *n*=3 independent experiments). All results are shown as Mean ± s.e.m.

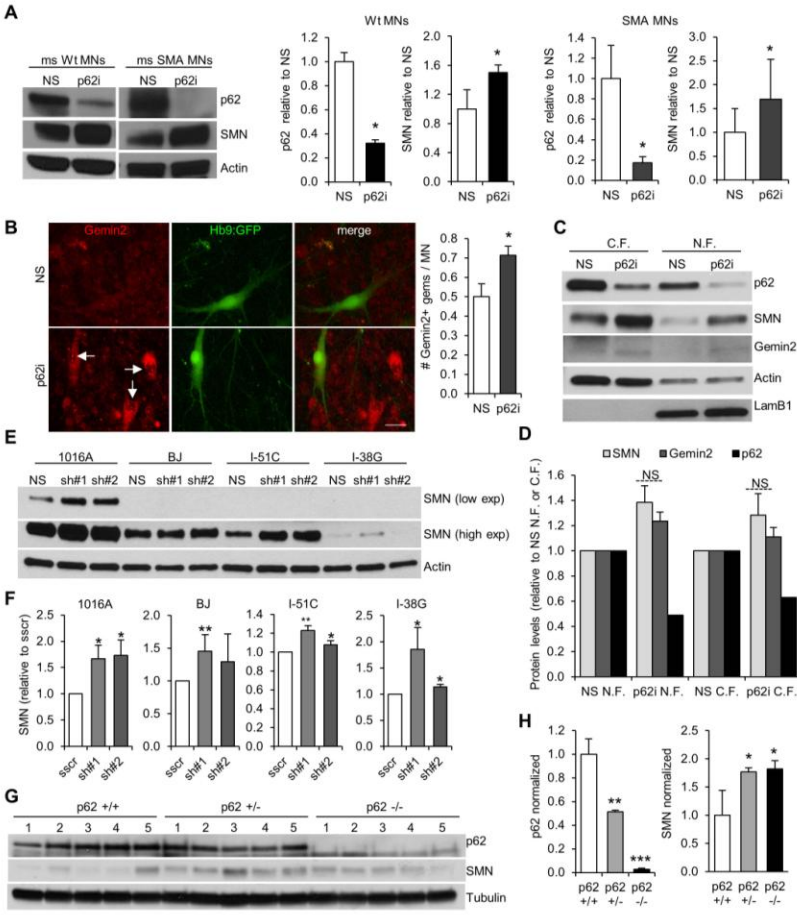

Figure 2. SMN degradation by autophagy is specifically mediated by p62. (A) Representative immunoblot from protein lysates from wildtype and SMA mouse ESC-derived MNs 7 days after being infected with non-silencing control (NS) or shRNA against p62 (p62i), and quantification of p62 and SMN protein levels shown on the right (Results expressed relative to non-silenced (NS)-control cells. Two-tailed *t*-test, *n*=5 independent experiments). (**B**) Immunostaining against gemin2 and quantification of the number of gemin2^{+} nuclear gems in SMA mouse ESC-derived MNs. Scale bar, 25 µm (Results expressed relative to NS-control cells. Two-tailed *t*-test, *n*=3 independent experiments. 600 MNs per condition were counted). (**C**-**D**) Representative immunoblot and quantification from subcellular fractionation 3T3 protein lysates 6 days after infection with lentivirus carrying shRNA against p62 or NS-control (NS, not significant). (**E**) Representative immunoblot from human iPSC-derived MN lysates from healthy control (1016A and BJ) and SMA patients affected with different disease severities (type II, I-51C; type I, I-38G). MNs were infected with lentivirus expressing NS shRNA control or p62 shRNA and lysed 7 days after infection. Quantification of SMN and p62 protein levels are shown in (**F**) (Results expressed relative to scramble (sscr)-silenced cells. Two-tailed *t*-test, *n*=7, 6, 4, 3 independent experiments from left to right). (**G**-**H**) Representative immunoblot and quantification from protein lysates obtained from p62 null (p62-/-), heterozygotes (p62+/-) or wildtype (p62+/-) adult mouse brains (Results expressed relative to p62+/+ mice. Two-tailed *t*-test, *n*=5 mice per group). All results are shown as Mean ± s.e.m.

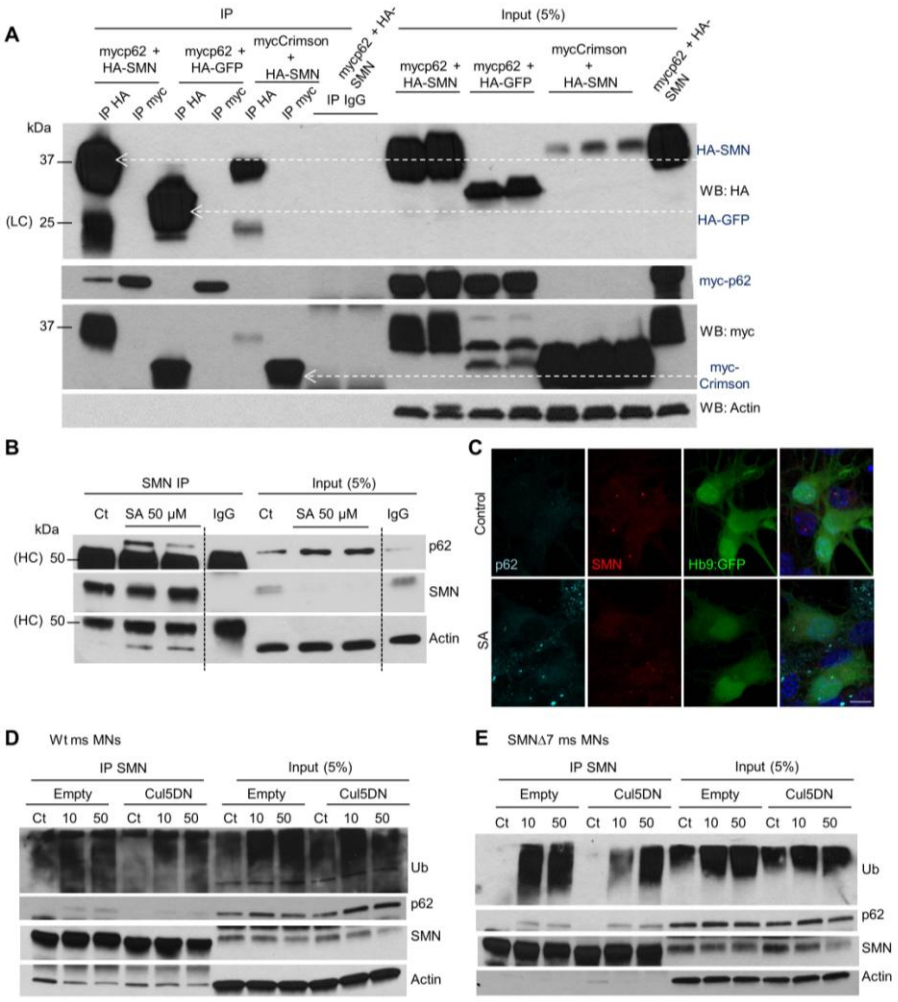

Figure 3. p62 interacts with SMN. (**A**) HA and myc representative immunoprecipitation from HEK293T lysates transfected with the indicated plasmids and immunoblotted against HA, myc and p62. (HC, heavy IgG chain; LC, light IgG chain). (**B**) Representative immunoprecipitation of endogenous SMN protein from mouse SMA MN lysates treated with control or sodium arsenite (SA) for 6 hours and immunoblotted against p62, SMN, LC3 and actin. (HC, heavy IgG chain; LC, light IgG chain). (**C**) Representative image from mouse SMA ESC-derived MNs cultured in control conditions or with SA and immunostained against p62 (cyan) and SMN (red) (MNs express Hb9:GFP and nuclei are stained with DAPI, blue). Scale bar, 10 µm. (**D**) Representative immunoprecipitation of endogenous SMN protein from mouse wildtype and SMA (**E**) MN lysates infected with lentivirus expressing the dominant-negative (DN) form of Cullin5 for 5 days compared to empty vector infected cells. MN cultures were treated with control media or SA (10 or 50 µM) the last 6 hours of the culture. Membranes were immunoblotted against ubiquitin, p62, SMN and actin.

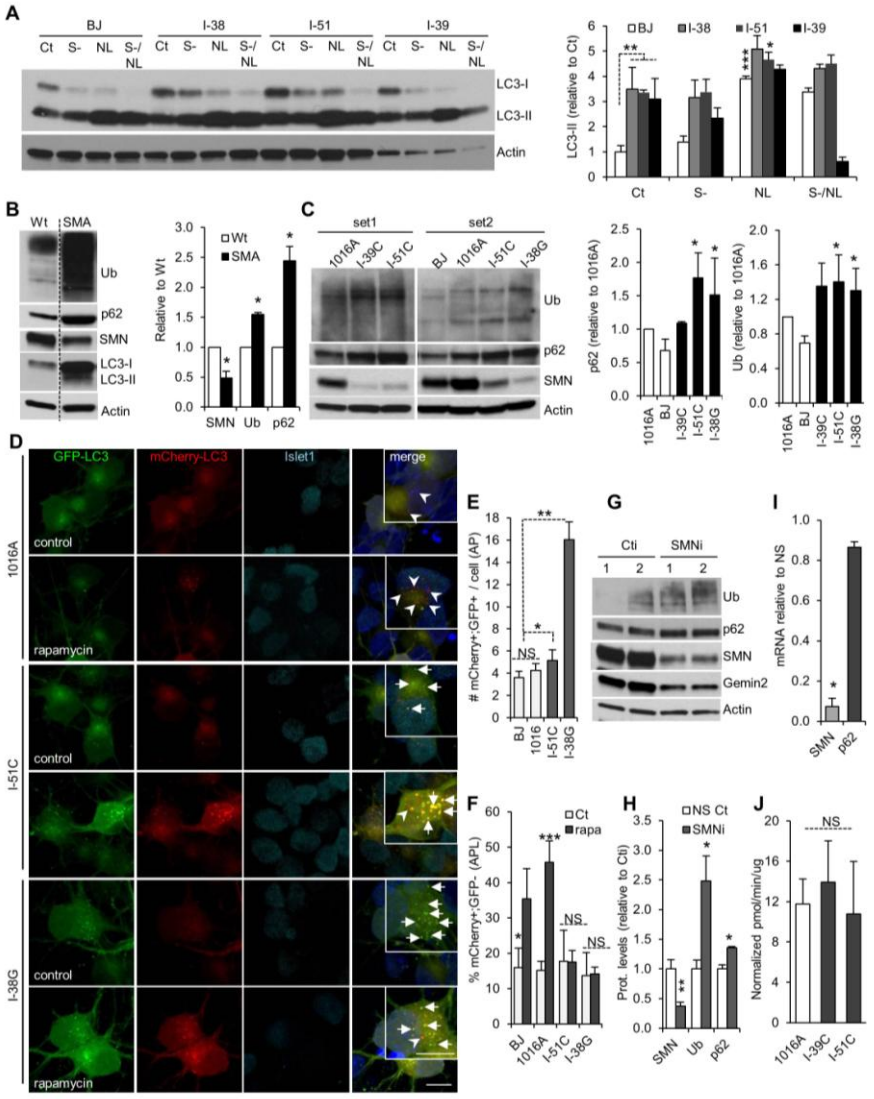

Figure 4. Autophagy activity is impaired upon SMN deficiency. (**A**) Representative immunoblot to determine autophagy flux from human control and SMA fibroblast protein lysates. Cells were treated in presence or absence of serum (S-) for 24 hours, with or without lysosomal inhibitors (NL, ammonium chloride plus leupeptin) the last 4 hours of the culture. Right, quantification of LC3-II levels. (**B**) Representative immunoblot of protein lysates from wildtype and SMA mouse ESC-derived MNs. Right, quantification (Results expressed relative to wildtype MNs. Two-tailed *t*-test, *n*=3 independent experiments). (**C**) Representative immunoblot from human iPSC-derived MN lysates from controls (1016A and BJ) and SMA patients affected with different disease severities (type III, I-39C; type II, I-51C; type I, I-38G). Right, quantifications (Results expressed relative to 1016A control MNs. Two-tailed *t*-test, *n*=5 independent experiments). (**D**) Representative confocal images of human control and SMA iPSC-derived MNs infected with mCherry-GFP-LC3 lentivirus. MNs were fixed 8 days after infection. Magnifications are shown in the insets. Scale bars, 10 µm. Quantification of the number of autophagosomes (APs, yellow, marked by arrows) and the percentage of autophagolysosomes (APLys, red, marked by arrowheads) (**E-F**) (Two-tailed *t*-test. 146, 44, 114 and 86 transduced MNs were counted for BJ, 1016A I-51C and I-38G, respectively). (**G**)

Representative immunoblot from HEK293T cells transfected with SMN RNAi or control RNAi for 3 days (duplicates are shown) and (**H**) quantification of protein levels (Results expressed relative to NS-control cells. Two-tailed *t*-test, *n*=3 independent experiments). (**I**) qPCR showing p62 mRNA expression upon SMN RNAi-mediated knock-down in HEK293T cells. Gene expression indicated as fold change of 2-ΔΔCt with respect to actin, normalized to RNAi-control cells (Results expressed relative to NS-control cells. Two-tailed *t*-test, *n*=2 independent experiments). (**J**) Quantification of the chymotrypsin-like activity in control versus SMA human MNs (NS, not significant). All results are shown as Mean ± s.e.m.

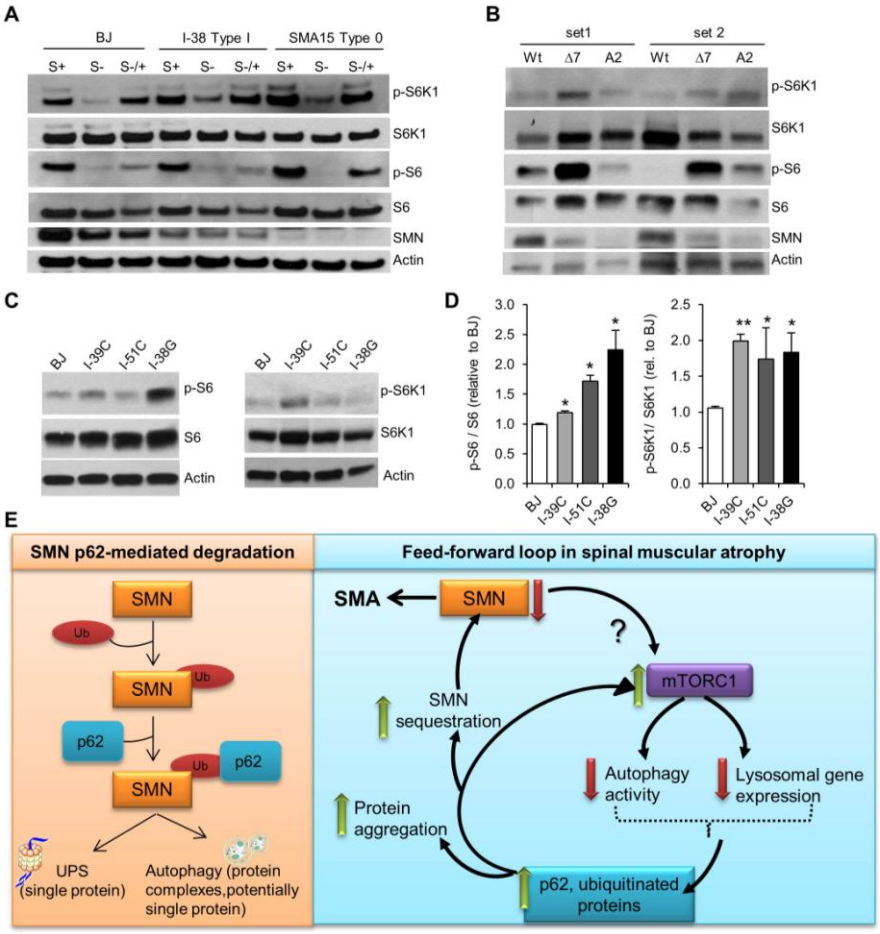

Figure 5. SMN deficiency results in mTOR activation which could contribute to the autophagy impairment observed in SMA cells. (A) Representative immunoblot from human healthy control and SMA types I and 0 fibroblasts lysates. Cells were cultured in the presence of 10% serum (S+), deprived of serum for 16 hours (S-) or deprived of serum and then incubated for an additional 30 min with serum (S-/+). Phosphorylated and total levels of mTOR targets S6K1 and S6 were measured. Quantifications are shown on Figure S4A. (**B**) Representative immunoblot from mouse wildtype and SMA (SMNΔ7 and A2) MN lysates to measure mTOR pathway. Quantifications are shown on Figure S4B. (**C**) Representative immunoblot from human healthy control and SMA MN lysates to measure mTOR pathway. (**D**) Quantifications of p-S6 to S6 and p-S6K1 to S6K1 ratios from human healthy control and SMA MN lysates (Mean ± s.e.m. expressed relative to BJ healthy control MNs. Two-tailed *t*-test, *n*=6 independent experiments). (**E**) Scheme of the interplay between low SMN–p62–mTOR–defective autophagy.

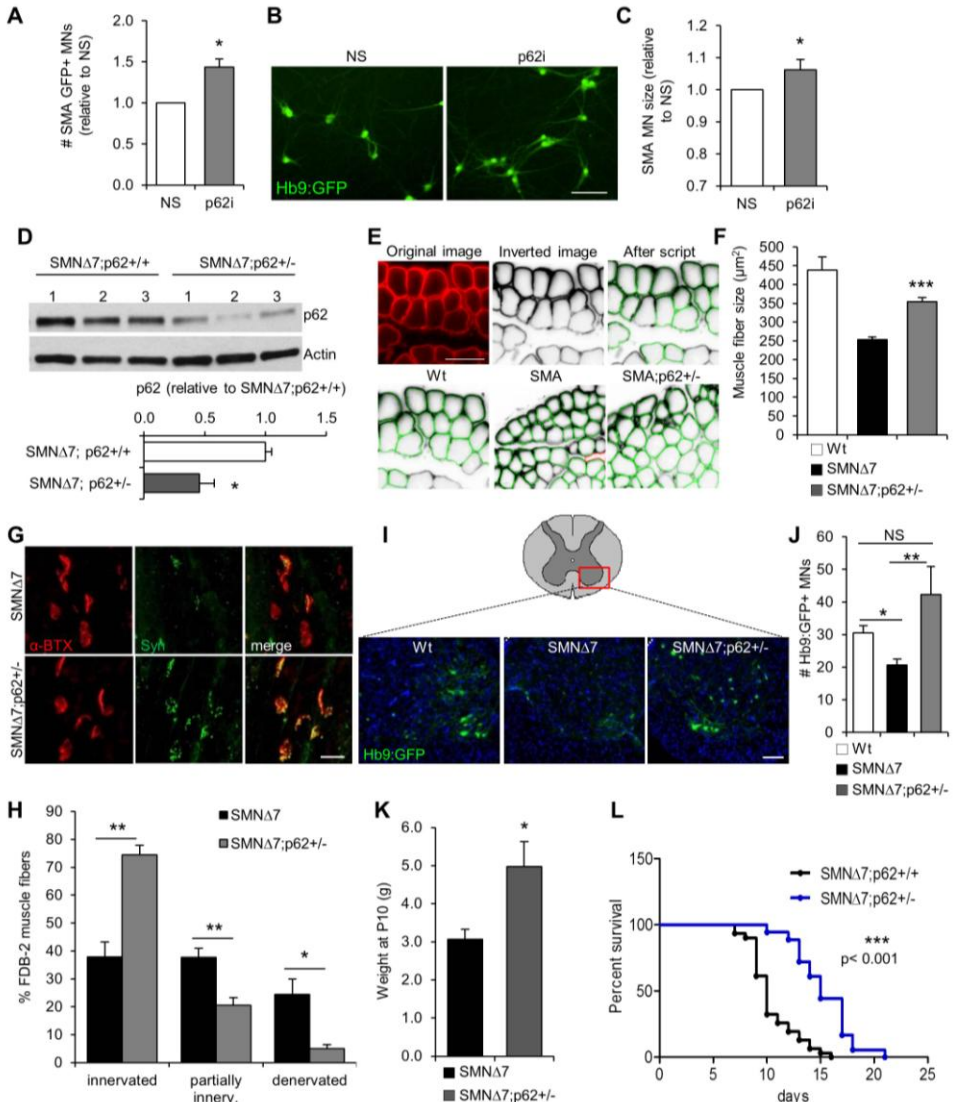

Figure 6. p62 knock-down promotes MN survival *in vitro* and ameliorates the disease phenotype of SMA models *in vivo*. (**A**) Quantification of Hb9:GFP^{+} SMA mouse ESC-derived MNs 9 days after infection with p62 shRNA lentivirus compared to the non-silencing (NS)-infected cells (Results expressed relative to NS-MNs. Two-tailed *t*-test, *n*=6 independent experiments) and (**B**) representative image. Scale bar, 50 μm. (**C**) Quantification of SMA MN soma size after p62 knock-down (Two-tailed *t*-test, 4100 NS and 5500 p62i MNs measured). (**D**) Representative immunoblot and quantification of spinal cord protein lysates from SMNΔ7 mice and SMNΔ7 hemizygotes for p62 (Two-tailed *t*-test, *n*=5 SMNΔ7;p62+/+, 3 SMNΔ7;p62+/- mice). (**E**) Representative images of cryosectioned TA muscles. Upper panels: original image showing laminin immunostaining (red), signal inverted by Columbus script and individual muscle fibers recognized by the script highlighted in green. Bottom panels, TA sections from wildtype, SMNΔ7 and SMNΔ7,p62+/- P10 mice. Quantification of TA fiber size (**F**). Scale bar, 50 μm. (Two-tailed *t*-test, *n*=5 wildtype, 4 SMNΔ7, 4 SMNΔ7;p62+/- mice). (**G**) Immunofluorescent images of SMNΔ7 and SMNΔ7,p62+/- FDB-2 P10 muscles showing NMJs immunostained for nerve terminals (anti-synaptophysin, green) and endplates (α-bungarotoxin, red). Quantification of fully innervated, partially, or fully denervated endplates (**H**). Scale bar, 20

µm. (Two-tailed *t*-test, *n*=4 SMNΔ7, 4 SMNΔ7;p62+/- mice). (**I**) Representative images from cervical spinal cord cryosections from P10 wildtype, SMNΔ7 and SMNΔ7;p62+/- mice showing Hb9:GFP^{+} MNs (nuclei stained with DAPI; central canals outlined with dotted circles). Average number of MNs per section (**J**). Scale bar, 100 µm. (Two-tailed *t*-test, n=10 wildtype, 9 SMNΔ7, 4 SMNΔ7;p62+/- mice). (**K**) P10 mice weight measurement (Two-tailed *t*-test, n=12 SMNΔ7, 8 SMNΔ7;p62+/- mice). (**L**) Kaplan-Meier plot showing survival curves for SMNΔ7 (black line) and SMNΔ7;p62+/- (grey dotted line) mice (Mantel-Cox and Gehan-Breslow-Wilcoxon tests, *n*=31 SMNΔ7, 18 SMNΔ7;p62+/- mice). All results are shown as Mean ± s.e.m.